Zn-Ti-Al layered double hydroxides synthesized from aluminum saline slag wastes as efficient drug adsorbents

L. Santamaría [a], M. López-Aizpún[a], M. García-Padial[a], M.A. Vicente [b], S.A. Korili [a], A. Gil [a,*]

[a]*INAMAT-Departamento de Ciencias, Edificio de los Acebos, Universidad Pública de Navarra, Campus de Arrosadía E-31006 Pamplona, Spain*

[b] *GIR-QUESCAT, Departamento de Química Inorgánica – Universidad de Salamanca, E-37008 Salamanca, Spain*

ABSTRACT

This work reports the synthesis of Zinc-Titanium-Aluminum (ZnTiAl) layered double hydroxides (LDH) with various proportions of Al-Ti and a Zn/(Al-Ti) molar ratio of 3:1 by the co-precipitation method. Two series, made with commercial aluminum (Al) and aluminum extracted from saline slags (Al*), have been considered. Structural characterization and comparison of the two series has been made using powder X-ray diffraction (PXRD), Nitrogen physisorption at 77 K, Scanning electron microscopy (SEM), X-ray photoelectron spectroscopy (XPS) and Thermogravimetry measurements. The adsorption capacity of diclofenac and salicylic acid, as examples of emergent pollutants, by the different LDH on batch and fixed-bed column experiments has been analyzed. The effect of various parameters, such as the pH, the initial concentration of pollutant, the mass of adsorbent and the contact time, on the sorption behavior were studied and compared. The contact time to attain equilibrium for maximum adsorption was found to be between 100 – 400 min. The kinetic and equilibrium results were correlated to several adsorption and isotherm equation models. The synthesized materials were more effective in removing diclofenac than salicylic acid, being $Zn_6Al^*_2$ the hydrotalcite that showed the highest adsorption capacity. The results showed a new application of a material obtained from the valorization of an industrial waste such as aluminum saline slags.

Keywords: aluminum industrial wastes, adsorption removal of diclofenac, hydrotalcite from saline slags, layered double hydroxides, adsorption removal of salicylic acid.

* Corresponding author. Tel.: +34 948 169602.

E-mail address: andoni@unavarra.es (A. Gil)

1. Introduction

Secondary aluminum refers to aluminum that is produced from recycled aluminum. The process of recycling aluminum has proven to be very cost-effective as it only uses between 5% and 20% of the energy needed for the production of primary aluminum and emits barely 5% of the greenhouse gas (Krammer, 2011; Tsakiridis, 2012); besides, the savings in raw materials should be taken into account. However, during the secondary aluminum smelting processes, aluminum saline slags are generated. These materials have been classified as hazardous wastes and as such must be deposited in secure deposits as their landfill disposal is forbidden in most European countries (European Waste Catalogue and Hazardous Waste List, 2002). Due to their heterogeneous composition, their applications are limited, with one of the most promising ones being the recovery of aluminum as a high-value-added product (Gil and Korili, 2016).

Non-steroidal anti-inflammatory drugs (NSAIDs) are water pollutants of increasing concern due to its proven presence in wastewater (Luo et al., 2014; Mompelat et al., 2009). Among them, diclofenac and salicylic acid are usually detected in water waste sediments, or even in drinking water samples (Carmona et al., 2014; Vulliet and Cren-Olivé, 2011). Several compounds have different removal efficiencies in wastewater treatment plants (Korma and Lambropoulou, 2014), and a low removal efficiency combined with a high ecotoxicity has resulted in diclofenac to be included in the European Commission's watch-list of substance for monitoring in the field of water policy 2015/495 (2015). Diclofenac in extremely low concentrations, lower than 1 μg/L, has been proven to change the liver ultrastructure of rainbow trout, to impair osmoregularity ability of a green shore crab and to significantly increase lipid peroxidation of zebra mussel, among other harms (Eades and Waring, 2010; Feito et al., 2012; Haap et al., 2008; Nassef et al., 2010; Quinn et al., 2011; Triebskorn et al., 2007). Salicylic acid was also found to be ecotoxic, although in greater concentrations than diclofenac (Caminada et al., 2006; Ginebreda et al., 2010).

The best ways to remove these toxic and persistent organic compounds from water has been examined with various procedures such as Fenton processes (Bautista et al., 2008), membrane processes (Radjenovic et al., 2008), flocculation (Suarez et al., 2009), photocatalysis (Santamaría et al., in press) or adsorption (Gil et al., 2019). Adsorption methods are among the most popular due to their low cost, their capacity to adsorb several types of pollutants and their simple and versatile use (Khenniche and Aissani, 2010).

Layered double hydroxides (LDH) are composed of positively charged brucite-like layers with negatively-charged balancing ions in the interlayer regions. They are also known as hydrotalcite-like compounds, because of the structural similarity to the natural occurring Hydrotalcite mineral, with formula $Mg_6Al_2CO_3(OH)_{16}\cdot 4H_2O$. LDH can be easily synthesized in laboratory where Mg^{2+} and Al^{3+} can be substituted for a large variety of Me^{2+} and Me^{3+} metallic cations. Although believed to be synthetic, recent discoveries have found a natural occurring Zn-Al-CO_3 mineral in Italy and Spain (Lozano et al., 2012). LDH are usually used as precursors for fabricating mixed metal oxides (MMO). By calcination at enough temperature, the structure collapses as CO_3^{2-} and H_2O disappear from the interlayer. If the calcination temperature is not excessively high, the resulting solids show, in the presence of water, a significant feature of LDH, the so-called "memory effect", and their original lamellar structure is recovered. In a Zn-Al LDH, zinc aluminum hydroxide hydrate is then formed, where the LDH is intercalated with OH^- as compensating ions in the interlayer (Kikhtyanin et al., 2017). This new compound has been proven to have unique characteristics such as intercalation, topological transformation and self-assembly (Li et al., 2014) to be used both as adsorbent and catalyst (Goh et al., 2008; Mohapatra and Parida, 2016). The presence of metals in the LDH structure opens the opportunity of new applications and can control/modify the existents. Several investigators have focused their research work on modifying the structure of TiO_2 to make it most sensitive, such as doping with transition metals or other elements (Gil et al., 2017; Santamaría et al., in press). The incorporation of Ti in the structure of LDH materials can improve the potential of these materials in applications to waste water treatments (Gao et al., 2011; Gomes Silva et al., 2009; Mendoza-Damián et al., 2013; Shao et al., 2011; Xia et al., 2013).

The use of LDH for the removal of pollutants by adsorption has been explored by several groups, mainly focusing their attention on the removal of anionic pollutants, from simple anions (chromate, phosphate, nitrate, arsenate, etc.) to organic contaminants containing at least one anionic group (carboxylate, sulphonate, phosphonate, etc.) such as surfactants, dyes, herbicides, and pesticides (Costantino et al., 2013; Ulibarri et al., 2001). Other strategy involving LDH for the decrease of the amount of contaminants in soils and waters consists on the preparation of controlled-release formulations, which supply fertilizers, plant nutrients, pesticides, and herbicides in agriculture in a more appropriate way (Costantino et al., 2013). This strategy has also been studied for the preparation of

controlled-release formulations of medicines (Rives et al., 2014). However, the use of hydrotalcites as adsorbents for the control of emerging pollutants has been less explored. In the particular case of salycilic acid, Silion et al. (2009) have reported its intercalation in LDH solids, and also Haraketi et al. (2016), who studied its controlled release, while Gualandi et al. (2011) have reported its removal by electrocatalytic oxidation using a Pt electrode coated with a Co/Al hydrotalcite, while up to our knowledge, its adsorption by LDH materials from aqueous solutions has been only reported by Elhalil et al. (2018). In the case of diclofenac, its intercalation in LDH has been reported by Heraldy et al. (2016) and San Román et al. (2012), while Ambrogi et al. (2002) studied its controlled release, and Khatem et al. (2015) and Boukhafa et al. (2017) have studied its adsorption from aqueous solutions using these materials.

The main objective of this work was the use of aluminum solutions (Al*) obtained from alkaline extraction of saline slag wastes as aluminum source for the synthesis of ZnAlTi hydrotalcites by a co-precipitation method. Zinc, as the Me^{2+} metallic cation, and a combination of Al-Ti in several proportions, as the Me^{3+} metallic cation, were used. Although the use of aluminum slags as a source for the preparation of hydrotalcite type solids has been recently explored (Gil and Korili, 2016; Gil et al., 2018), up to our best knowledge the preparation and use of ZnAlTi-LDH from this resource have not been reported elsewhere. Commercial aluminum solutions (Al) were also used for comparison purposes. The synthesized and calcined LDH were then considered as adsorbents for the removal of diclofenac and salicylic acid, as representative compounds of emergent pollutants. This method of preparation of materials and their use may confer an important applicability, not previously reported, to aluminum saline slags.

2. Experimental procedure

2.1 Materials

The materials used for the synthesis of hydrotalcites were: $Zn(NO_3)_2 \cdot 6H_2O$ (≥98%, Sigma-Aldrich), Na_2CO_3(≥99.99%, Sigma-Aldrich), $TiCl_3$(≥12%, Sigma-Aldrich), NaOH (Panreac) for pH adjustment and aluminum extraction, and $Al(NO_3)_3 \cdot 9\ H_2O$ (≥95%, Merck). Salicylic acid, (2-hydroxybenzoic acid, 2-$(HO)C_6H_4COOH$, ≥99.99%, Sigma-Aldrich) and diclofenac sodium salt (2-[(2,6-dichlorophenyl)amino]benzeneacetic

acid sodium salt, $C_{14}H_{10}Cl_2NNaO_2$, Sigma-Aldrich) were also used without any modification.

2.2 Hydrotalcite-like compounds synthesis

Al* was extracted from aluminum saline slags using the following procedure: 5 g of saline slag were added to 100 mL of an aqueous reagent solution (NaOH 2 mol/L) in a reflux system, stirred at 500 rpm and heated to 373 K for 60 min. The slurries were separated by filtration and the aluminum concentration in the solution was determined by ICP-OES and found to be 7.03 g/L.

Hydrotalcites were synthesized on a Zn^{2+}:(Al, Ti)$^{3+}$ 3:1 molar ratio utilizing the co-precipitation method, with aluminum and titanium proportions being modified in the series. As an example, $Zn(NO_3)_2 \cdot 6H_2O$ (0.15 mol/L), Al* (0.0375 mol/L) and Ti^{3+} (0.0125 mol/L) were added dropwise to Na_2CO_3 (0.015 mol/L) to a final volume of 400 mL. NaOH was used during the process to adjust the pH to 10. The mixture was stirred at 500 rpm and 333 K for 60 min and aged for 24 h. The slurries obtained were centrifuged at 8000 rpm for 5 min and washed. This process was repeated several times until the washing water achieved a pH of 7. The samples were then dried at 353 K for 16 h, manually grounded with a mortar and calcined at 673 K for 4 h. The nomenclature used for the samples was $Zn_6Al_xTi_y$, with x+y= 2 to maintain the 3:1 ratio. The same series were synthesized using commercial and extracted aluminum.

2.3 Characterization of the adsorbents

The textural properties of the samples (0.4 g) were analyzed by nitrogen (Praxair, 99.999%) adsorption-desorption at 77 K (Micromeritics ASAP 2020 Plus adsorption analyzer). All samples were degassed beforehand at 423 K for 24 h under a pressure lower than 0.1 Pa. The specific surface area (SSA) of the materials was estimated by the Brunauer-Emmer-Teller (BET) method applied to a relative pressure range of 0.05 – 0.20. The external surface area (S_{ext}) and the micropore volumes ($V_{\mu p}$) were also estimated using the t-plot method.

The crystalline phase of the samples was identified by powder X-ray diffraction (PXRD) using a Siemens D-5000 X-ray diffractometer with Ni-filtered Cu Kα radiation (λ = 0.1548 nm) in a 2θ range from 5 to 80° and a scanning rate of 0.2° (2θ)/min.

Scanning electron microscopy (SEM) was used to analyze the morphology of the samples (JEOL, JSM-6400 instrument operating at 20 kV).

X-ray photoelectron spectroscopy (XPS) analyses were carried out on a SPECS Phoibos 150 1DDLD spectrometer equipped with an Al Kα source of 1486.7 eV. The surface adventitious carbon peak, C 1s at 284.8 eV, was used as a reference for all the binding energies. Acquisition parameters and sensibility factors provided by the manufacturer were used to normalize peak areas and calculate surface concentrations (% atomic).

Thermogravimetric measurements were performed on a Hi-Res TGA2950 apparatus (TA-Instruments) using a 10 K/min heating rate from room temperature up to 1173 K under an air atmosphere (60 mL/min).

The salt addition method was used to determine the point of zero charge. A 0.01 mol/L NaCl solution was used as background electrolyte. An equal quantity of background solution (50 mL) was apportioned into various flasks kept in series with increasing pH values from 2 to 12. 0.15 g of adsorbent were added to all these flasks and the change in pH of each solution was recorded after shaking the samples for 48 h. This change in pH was plotted against the initial pH values on the graph, and the PZC was identified as the pH when ΔpH = 0.

2.4 Adsorption procedure

2.4.1 Batch experiments

The adsorption of diclofenac and salicylic acid on the hydrotalcites was studied by determining the adsorption isotherms considering previous works of our research group (Gil et al., 2019). The effect of pH was considered up front. Drug solutions (25 μmol/L) were adjusted to a pH range of 2–12 using either HCl or NaOH, placed in a beaker with 50 mg of adsorbent and shaken for 2 h in a stirring plate at room temperature. The dispersions were then filtered (0.45 μmol, Durapore) and the pollutant concentration remaining in the solution was determined by a Jasco V-730 UV-Vis spectrometer at the

maximum absorption wavelength, 276 and 297 nm for diclofenac and salicylic acid, respectively.

In the kinetic tests, to study the effect of the drug concentration, 50 mg of adsorbent were added to 250 mL of solutions with drugs in varying concentrations of 25, 50 and 75 μmol/L. The effect of the adsorbent dose was examined by changing the amount of the adsorbent (25, 50 and 100 mg) in solutions with an initial drug concentration of 75 μmol/L. Throughout the duration of the experiments, samples were shaken in a stirring plate and the solution was sampled at various time intervals until equilibrium was achieved, up to 8 h. The quantity of organic compound adsorbed by the hydrotalcites was calculated from the difference between the initial and remaining concentrations according to the following equation:

$$q_{t,e} = \frac{V \cdot (C_0 - C_{t,e})}{m} \qquad \text{(Equation 1)}$$

where C_0 and C_t (μmol/L) were the initial and final concentrations of organic compound in solution, respectively, V (mL) was the volume of the solution and m (g) was the adsorbent mass.

To describe the transport to adsorbates inside adsorbent particles, several kinetic modelling approaches can be considered; in this study pseudo-first- and pseudo-second-order rate equations were applied using OriginPro program (version 9.0) to test the experimental data.

$$\frac{dq}{dt} = k_1 \, (q_e - q_t) \qquad \text{(Equation 2)}$$

$$\frac{dq}{dt} = k_2 \, (q_e - q_t)^2 \qquad \text{(Equation 3)}$$

where q_e and q_t (μmol/g) were the amounts of solute adsorbed at equilibrium and at a certain time, t, respectively, k_1, and k_2 were the reaction rate constants of pseudo-first and pseudo-second-order rate, respectively. Equations 2 and 3 are obtained considering mass balances to the liquid phase in the batch system and assuming the kinetic models inducted

for the driving force. After integration, the well-known equations for pseudo-first and pseudo-second-order kinetic models are found.

The adsorption capacity of the hydrotalcites in equilibrium was tested by modifying the initial drug concentration. 5 mg of adsorbent were added to glass tubes containing 10 mL of the contaminant solution at initial concentrations between 0 and 1000 μmol/L. The tubes were shaken for 8 h and the concentration of the pollutant remaining in the solution was separated from the solid by filtration and the remaining concentration determined by UV–visible spectrophotometry as in the case of the adsorption kinetic experiments. The amount of organic compound adsorbed per unit mass of adsorbent at equilibrium was determined according to Eq. (1), where C_e (μmol/L) was the concentration of that compound at equilibrium.

The equilibrium experimental data obtained were used to better interpret the interactive behavior between solutes and adsorbents, considering three equilibrium adsorption isotherms: Freundlich, Langmuir and Toth.

$$q_e = k_F \cdot C_e^{1/m_F} \quad \text{(Equation 4)}$$

$$q_e = \frac{k_L \cdot q_L \cdot C_e}{1 + k_L \cdot C_e} \quad \text{(Equation 5)}$$

$$q_e = \frac{k_T \cdot q_T \cdot C_e}{[1 + (k_T \cdot C_e)^{m_T}]^{1/m_T}} \quad \text{(Equation 6)}$$

where q_e (μmol of adsorbate/g of adsorbent) was the amount adsorbed, C_e (μmol/g) was the monolayer capacity, k_i the equilibrium constant (k_F) or the binding affinity (k_L, k_T) and m_i characterized the mobility of the molecules adsorbed and the heterogeneity of the system.

The adsorption process in porous adsorbents was also examined with the estimation of the effective diffusion coefficient by applying a fractional approach to the equilibrium, *F(t)* (Khraisheh et al., 2002):

$$F(t) = \frac{C_0 - C_t}{C_0 - C_e} = \sqrt{1 - exp\left(-\frac{\pi^2 D t}{r^2}\right)} \quad \text{(Equation 7)}$$

where D (m^2/s) is the intraparticle-diffusion coefficient and r (m) is the particle size radius assuming a perfect sphere.

2.4.2 Fixed-Bed adsorption experiments

The breakthrough curves of diclofenac and salicylic acid were performed on a column of 2 cm in diameter and 12 cm long packed with silicon carbide (0.5 mm) and 25 mg of hydrotalcites, in order to complete the volume and avoid dead volume. A solution containing 20 µmol/L of the organic molecules was fed at a flow of 0.2 mL/min using a peristaltic pump (Ecoline VC-380) in down-flow mode. The effluent from each column was collected at various time intervals up to 120 minutes and the amount of remaining pollutants was quantified by means of ultraviolet-visible absorption spectrophotometry, as previously described for the batch experiments. The results were adjusted to the Thomas model which allows for a simple interpretation of the behavior inside the column. This model takes into account only direct adsorption in the unused capacity of the adsorbent and ignores the intraparticle mass transfer resistance and the external resistance (i.e. the adsorbate adsorbed onto the solid surface directly) (Poulopoulos and Vassilis, 2006).The non-linearized Thomas equation (Thomas, 1944) can be expressed as follows:

$$\frac{C_t}{C_0} = \frac{1}{1+\exp(\frac{k_{Th}q_{ads}m}{Q} - k_{Th}C_0t)} \qquad \text{(Equation 8)}$$

where C_0 (µmol/L) and C_t (µmol/L) were the influent and effluent adsorbate concentration, respectively, at a time t, m was the mass of the adsorbent (g), Q was the volumetric flow rate (mL/min), k_{Th} (mL/min·µmol) was the Thomas rate constant and q_{ads} (µmol/g) was the equilibrium adsorbate uptake per g of the stabilized system.

3. Results and discussion

3.1. Hydrotalcites characterization

The powder X-ray diffraction patterns of the non-calcined and calcined samples can be seen in Fig. 1. First, a study was conducted on how pH could affect the synthesis of

the hydrotalcite. The relevance of the pH throughout the synthesis is shown in Fig. 1a, when keeping the pH stable at 10 during the process, a layered double hydroxide type structure was formed (marked as 1). A no crystalline structure or a mixture of hydrotalcite and zincite (ZnO, marked as 2) was found when the synthesis pH was lower (pH = 5) or higher (pH = 12) than 10. When calcined, the structure collapsed and zincite appeared at pH 10 and 12 (see Fig. 1b). PXRD diffraction patterns of the non-calcined samples synthesized from commercial aluminum (Al) and extracted aluminum (Al*) were compared in Figs 1c and 1d. The crystallinity decreased with the increase of the titanium content and no diffraction reflections corresponding to titanium compounds were observed in the XRD patterns, suggesting that titanium was incorporated into the octahedral positions of the LDH or well dispersed into the LDH structure. The distinct basal (003) reflection, characteristic of hydrotalcite-like materials, was found at around 11.7º. The *c* parameter was calculated using the reflection (003) values, $c = 3d_{003}$, with *c* corresponding to three times the basal value (see Table 1). Several factors can affect the *c* parameter (Mendoza-Damián et al., 2013). The results found in this work can be related to the effect of the substitution of Al^{3+} by titanium, modifying the interaction between the brucite-like layer and the interlayer. *d* had a value of around 0.76 nm in the four first samples which accorded well to other experimental results for ZnAl-LDH with carbonated anions (Fraccarollo et al., 2010). In the case of Zn_6Ti_2, the small basal value suggested that the hydrotalcite structure was not properly formed. From the experimental results obtained, both series of hydrotalcites synthesized were similar between them, with more defined hydrotalcite patterns when there was more aluminum in the sample. After calcination at 673 K, the structure was destroyed and zincite was found in all the cases (see Figs 1e and 1f, for Al and Al* samples). No diffraction reflections corresponding to TiO_2 phases, anatase or rutile, were observed suggesting a high dispersion of the oxides or a low crystallinity.

To test the memory effect, a study with the sample $Zn_6Al^*_2$ has been considered (see Fig. 2). The calcined sample $Zn_6Al^*_2$ was submerged in water for 2 h, dried at 353 K and the hydrotalcite structure (marked as 1) was recovered, but a part of zincite (marked as 2) also remained (see Fig. 2c). The elimination of the carbonates in the rehydration experiment lowered the basal value from 0.761 to 0.734 nm (see Table 1). Considering the thickness of the host layer to be 0.471 nm (Conterosito et al., 2013), that left the interlayer space, occupied by hydroxides in 0.263 nm as opposed to 0.291 nm when the

interlayer contained carbonates. An aqueous solution of 25 μmol/L of diclofenac and 1 g/L of calcined $Zn_6Al^*_2$ were also combined for 2 h and the XRD pattern showed a new distinctive reflection appearing at 8.05º (2θ degrees) (see Fig. 2d), corresponding to an interlayer height of 0.626 nm. The size of diclofenac was between 0.766 and 0.957 nm, thus the molecules were likely to be intercalated in an almost horizontal position between the layers (Brindley and Kao, 1984).

In order to further study the morphology of the samples, SEM analysis of the materials was performed (see Fig. 3). The characteristic flat structure with sharp edges evidenced that the layered structure remained after calcination, as reported elsewhere (Castro et al., 2011; Xie et al., 2006). The release of water and CO_2 and their replacement by hydroxyl groups did not drastically affect the crystal structure of the LDH. The addition of Ti^{3+} caused morphological modifications of the samples. As the proportion of titanium increased, the layered flat structure gradually disappeared to form rounder particles which were the only ones remaining in the Zn_6Ti_2 sample. These results were in accord to the XRD patterns. EDX analyses were also performed to determine the composition of the samples. No impurities were observed, however chlorine was found because titanium source was $TiCl_3$.

The N_2 adsorption-desorption isotherms of dried and calcined samples are presented in Fig. S1. According to the IUPAC classification, type II adsorption isotherms were observed in all the samples, related to the presence of nonporous or macroporous adsorbents. They all had a type H3 hysteresis loop, typical of non-rigid aggregates of plate-like particles (Thommes et al., 2015) with slit-shaped pores of non-uniform size and shape (Lowell et al., 2004). For the Al series (see Table 2), the maximum value of SSA corresponded to the sample made at pH = 5, while the minimum value corresponded to the sample obtained at pH = 12. For the samples synthesized at pH = 10, the nitrogen monolayer volume increased with the addition of titanium: Zn_6Al_2 sample has a S_{BET} of 81 m^2/g, when titanium was incorporated the SSA went up to between 142 and 190 m^2/g. Similar results were found for the Al* series (see Table 3). The results of external SSAs and micropore volumes confirm the non-porous character of the samples. Since the N_2 diameter is larger than the interlayer space for carbonate containing layered double hydroxides, the SSA measured by this method corresponded to the surface area. A well-defined hydrotalcite had better crystallinity and bigger particles, whereas poor crystalline samples were usually formed by smaller particles, where interactions between particles

were bigger, thus increasing the total surface (Albiston et al., 1996; Benito et al., 2006). Surface areas of LDH prepared with Al and Al* were in the same order, the maximum difference was found in $Zn_6Al_{1.5}Ti_{0.5}$: 142 m^2/g in the sample with Al and 152 m^2/g in the sample with Al*. When the samples were calcined, the SSA was decreased in all cases, except in Zn_6Al_2*sample. The samples synthesized at pH = 10 went from a range of 142-190 m^2/g to a range of 91-104 (Al) and from 152-199 m^2/g to 93-100 m^2/g (Al*). The SSA were more homogeneous after calcination. This surface decrease has been reported before (Hadnadjev-Kostic at el., 2013) as various types of LDH respond diversely to calcination (Cavani and Trifiro, 1991).

The thermogravimetric analysis of $Zn_6Al_2CO_3(OH)_{16} \bullet 4H_2O$ has been reported by several authors (Frost et al., 2005; Theiss et al., 2013), with similar results to the samples included in this work (see Fig. 4). Five mass loss steps were observed and the results were summarized in Table 4. The first two mass losses, at less than 373 K and around 423 K, corresponded to the loss of water. Step 1 was associated with adsorbed water and step 2, always bigger than step 1, to the loss of interlayer water. The mass of water in Zn_6Al_2 was equal to 14.2%, with 12% in the form of interlayer water, which diminished in the series as the amount of titanium was increased. In the sample Zn_6Ti_2 water loss steps 1 and 2 were combined into one located around 373 K. This was due to the poor crystallinity of the sample, the hydrotalcite structure was limited thus there was no interlayer water. The third step, located at around 523 K, was the most intense in all the cases with the exception of Zn_6Ti_2. This step corresponded to a combination of dehydroxylation and decarbonation which, in the case of the sample without titanium, can be proposed as:

$$Zn_6Al_2CO_3(OH)_{16} \rightarrow Zn_6Al_2O_8CO_3 \rightarrow 6ZnO \bullet Al_2O_3$$

Step 4 and 5 were quite small and usually interpreted as the further decomposition of the mixed metal oxide. Results in the series prepared with Al* *vs* the series with Al were close, with a bigger percentage of water loss in samples with commercial aluminum and, consequently, a smaller one in dehydroxylation/decarbonation. Impurities brought with aluminum, which slightly decreases the crystallinity of the samples, could be responsible for a smaller interlayer surface.

XPS analysis were conducted to study the chemical states on the surface of the five samples with Al* and to further analyze the structure variation when Ti^{3+} was introduced. The main differences in theXPS spectra of the samples (Fig S2) can be found in the peaks for Al* and Ti. The surface concentration (% atomic) and elemental formula of the samples (see Table 5) were close to predictions, with a slight increase in the amount of aluminum. High resolution spectra of O 1s, Ti 2p, Zn 2p and Al 2p were shown in Fig. 5. Core level O 1s spectra were displayed in Fig. 5b. After the spectra deconvolution of Zn_6Al_2* three peaks were detected: O-metal at 531.14 eV bound to metal cations of the structure, hydroxide at 532.24 eV could appear due to a weak bonded surface oxygen and in the form of adsorbed water at 533.04 eV (Lu et al., 2012; Wang et al., 2015). As titanium was introduced in the structure, O 1s peaks shifted towards lower binding energies, this was due to two factors: the appearance of a Ti-O bond located at 530 eV (Moulder, 1992) moved towards the left the O-metal peak, and the decrease of adsorbed water in the interlayer made hydrotalcite structure less defined and reduced the peak located at the right. Zinc $2p_{3/2}$(Fig. 5a) peak was located in all cases near 1022 eV, and corresponded to ZnO (Xiong et al., 2019). There was no direct bond between zinc and titanium as no significant shift was found when titanium was introduced in the samples. Ti 2p (Fig. 5d) spectra showed how the intensity of the peaks increased with titanium proportion. Deconvolution of Zn_6Ti_2 formed two peaks at $2p_{3/2}$ corresponding to Ti^{4+} (459.1 eV) and Ti^{3+} (457.2 eV) and another two peaks at $2p_{1/2}$ at 464.8 and 463.0 eV for Ti^{4+} and Ti^{3+}, respectively. The molar percentage was calculated to be 14.7% of Ti^{3+} with Ti^{4+} accounting for the rest.

3.2 Adsorption experiments

3.2.1 Batch adsorption results

The adsorption process depended on several factors such as the pH of the solution, the adsorbent dose and the drug concentration. The pH effect was studied up front (Table 6). The best pH values for the adsorption of diclofenac and acid salicylic were 4.2 and 2.7, respectively, which were the pH of the aqueous solutions without any modification. For that reason, these pH values were chosen for the experiments. It was inferred from the Table that the more basic the pH was, the less amount of drugs was adsorbed.

The kinetic adsorption data for diclofenac and salicylic acid, respectively, on four hydrotalcites considering several drug concentrations and adsorbent amounts are presented in Fig. 6 and 7. Sample Zn_6Ti_2 was not capable of adsorbing any of the anti-inflammatory drugs. The effect of the adsorbent was studied (first columns of Fig. 6 and 7), considering several quantities: 25, 50 and 100 mg of adsorbent in 0.25 L of water and 75 μmol/L of drug. The experiments on diclofenac showed the decrease of the adsorption capacity with the increase of adsorbent concentration. This might be due to the partial overlapping or aggregation of adsorption sites when the amount of adsorbent was raised, which produced a reduction in the available specific surface area (Gil et al., 2019). There was a great difference in the adsorption capacity between the samples. With a 100 mg/L concentration of adsorbent, its adsorption capacity ranged from 38 μmol/g in $Zn_6Al^*_{0.5}Ti_{1.5}$ to more than 409 μmol/g in $Zn_6Al^*_2$. In the case of salicylic acid, the adsorption capacity also changed, from 7 μmol/g ($Zn_6Al^*_{0.5}Ti_{1.5}$) to 80 μmol/g ($Zn_6Al^*_2$). The results when the initial drug dose was modified were shown in the second columns. The quantities of diclofenac and salicylic acid considered ranged from 25 to 75 μmol/L and the amount of adsorbent was 50 mg, i.e. 200 mg/L, in all the experiments. In this case, an increase in the initial drug dose favored its adsorption. This was because each adsorbent had the capacity to adsorb a fixed amount of adsorbate species. Until this amount was reached, an increase in the adsorbate concentration meant an increase in the adsorption capacity of the adsorbate. Comparing the adsorbates, the diclofenac adsorption capacity of $Zn_6Al^*_2$ was the greatest (more than 250 μmol/g with a 75 μmol/L initial dose of adsorbate) and went down until 30 μmol/g for $Zn_6Al^*_{0.5}Ti_{1.5}$. For the salicylic acid, these amounts went from 87 to 10 μmol/g, respectively.

The capacity of the samples to adsorb diclofenac and salicylic acid can be explained by means of the point of zero charge values (7.5 – 7.7). A pH below the pH_{pzc} meant that the net charge of the adsorbent was positive and a pH above the pH_{pzc} the adsorbent was charged negatively. At the pH of the experiments (2.7 for salicylic acid and 4.2 for diclofenac) the adsorbents had a net positive charge in their surface. It has been proven that in both the salicylic acid and diclofenac adsorption a hydrogen bond between the COO^- and the hydroxyl groups occurred (Mosangi et al., 2016; Xiong et al., 2019), which can be responsible for overcoming the small electrostatic barrier. Considering the quantity of drug adsorbed, the amount of diclofenac adsorbed by the four studied hydrotalcites was higher than that for salicylic acid. Salicylic acid (see Table S1) had a benzene ring

attached to a hydroxyl group and, adjacent to it, a –COOH group was present. Being the carboxylic group an electron withdrawing group, it pulled electrons toward itself and forced the adjacent hydroxyl group to give up its electron and to get as proton released. This intramolecular hydrogen bond made salicylic acid less prone to bond with the adsorbent.

The adsorption capacity of the LDH decreased as titanium was incorporated into the structure. This was to be expected as the addition of titanium worsened the LDH structure (see PXRD and SEM results, Fig. 1 and 3) and less hydroxyl groups were found (see XPS results, Fig. 5). The possible effect of the micropores can be considered negligible from the micropore volumes estimated for these samples.

Pseudo-first- and pseudo-second-order rate equations were applied to the experimental data of Fig. 6 and 7, and k_1 and k_2 values are shown in Tables S2 and S3. In order to test the best correlation of the experimental data, chi-square (χ^2) and the coefficient of determination (R) were used. It seemed that the inclusion of data close to, or at, equilibrium to determine the best kinetic formula have introduced a methodological bias that has promoted pseudo-second-order kinetics as the number one model (Simonin, 2016). For this reason, sample collection was stopped once the equilibrium was achieved. The results thus revealed that the adsorption of both drugs can be best described as a pseudo-first-order linear reaction. When comparing k_1 values results, they were in accord to the experimental data, that is, k_1 constant increased with the increase of the initial drug concentration and decreased as the adsorbent concentration increased from 100 mg/L to 400 mg/L. The preference of any adsorbate to link to high energy sites, when available, resulted in faster reaction kinetics and, as these sites were occupied, lower energy ones will be taken which decelerated the process and could explain the evolution of the k_1 constants (Chu, 2002). The estimated effective diffusion coefficients (Table S4) indicated that the intraparticle diffusion had a low effect on the adsorption of diclofenac and salicylic acid by the ZnTiAl LDH. As a general effect, it was found that the diffusion coefficient decreased when the amount of adsorbent increased and tended to increase with the concentration of the pollutant used.

Once the equilibrium time was selected, the equilibrium adsorption isotherm of diclofenac on the $Zn_6Al^*_2$ hydrotalcite as adsorbent with a higher adsorption capacity was also plotted. Langmuir, Freundlich and Toth isotherm equations modeled the experimental data for diclofenac. The results are shown in Fig. S3 and the goodness of fit

of the models was evaluated with χ^2 and R (see Table 7). The adsorption isotherm can be related to a L-type behavior according to the classification proposed by Giles (1974). This behavior was related to a system in which the contaminant interacted strongly with the surface of the adsorbent. The three models fitted well with the experimental data although Toth represented the data with more accuracy.

3.2.2. Fixed-Bed adsorption results

Breakthrough behavior of the column adsorption process with diclofenac and salicylic acid on the Zn_6Al*_2 hydrotalcite was also investigated. The breakthrough curves obtained for the drugs were included in Fig. 8. Experimental results were adjusted considering the Thomas equation (see Table 8). R showed that the Thomas model had good adjustment to both drugs. The diclofenac molecule crosses the adsorbent bed at a faster rate than the salicylic acid molecule. There were a minor interaction with the adsorbent, which can be explained by the larger size of the diclofenac molecule compared to the size of the salicylic acid molecule (see Table S1). In the batch experiments the time to reach the equilibrium was high, between 100 and 400 min, so if the diclofenac molecule could diffuse into the adsorbent lattice, it had enough time to do so. In the case of these experiments, it was not possible so it is retained in a smaller proportion than salicylic acid.

Summary and conclusions

Herein, a new procedure for the recovery of aluminum present in saline slags generated during the secondary recycling processes of aluminum as an adsorbent of diclofenac and salicylic acid, as examples of emerging contaminants, has been reported. For this purpose, the aluminum extracted with aqueous NaOH solutions was used as an alternative source of aluminum for the synthesis of hydrotalcite-type ZnTiAl, with a molar ratio Zn/(Al + Ti) = 3 and several Al/Ti ratios, by a coprecipitation method at pH = 10. The uncalcined and without Ti samples evidenced the presence of the typical hydrotalcite structure with a high crystallinity from the XRD analyses. As the amount of Ti increased, the crystallinity of the samples decreased appreciably. After calcination at 673 K, the hydrotalcite structure was destroyed and zincite (ZnO) was found. The textural properties, namely the specific surface area, decreased with the calcination temperature, related to the presence of amorphous mixed oxides, while increased when incorporating

Ti into the structure from 78 to 199 m^2/g. By calcination of the samples at 673 K, these properties decreased due to the presence of amorphous mixed oxides. The presence of Ti in the LDH structure was confirmed by XPS analysis. All these characterization results were also confirmed by the synthesis of ZnTiAl LDH from aluminum nitrate as a commercial source.

The kinetic study of the adsorption process showed that 100-400 min were necessary for the emerging pollutants/hydrotalcites systems to reach the equilibrium. The hydrotalcites synthesized retained more diclofenac than salicylic acid (409 and 80 μmol/g, respectively), and the adsorption capacity was greater when Ti content in the adsorbents was lower. Zn_6Al_2solid was very effective in retaining this type of organic pollutants.

Acknowledgements

This work was funded by the Spanish Ministry of Economy, Industry and Competitiveness (AEI/MINECO), and the European Regional Development Fund (ERDF) through project MAT2016-78863-C2-R and the Government of Navarra through projects PI017-PI039 CORRAL. LS thanks Universidad Pública de Navarra for a pre-doctoral grant. AG also thanks Santander Bank for funding through the Research Intensification Program.

Appendix A. Supplementary data

Supplementary data to this article can be found online at https: XXX

References

Albiston, L., Franklin, K.R., Lee, E., Smeulders, J.B.A.F., 1996. Rheology and microstructure of aqueous layered double hydroxide dispersions. J. Mater. Chem. 6, 871–877.

Ambrogi, V., Fardella, G., Grandolini, G., Perioli, L., Tiralti, M.C., 2001. Intercalation compounds of hydrotalcite-like anionic clays with anti-inflammatory agents. II: uptake of diclofenac for a controlled release formulation. AAPS PharmSciTech 3, article 26.

Bautista, P., Mohedano, A.F., Casas, J.A., Zazo, J.A., Rodriguez, J.J., 2008. An overview of the application of Fenton oxidation to industrial wastewaters treatment. J. Chem. Technol. Biotechnol. 83, 1323–1338.

Benito, P., Labajos, F.M., Rocha, J., Rives, V., 2006. Influence of microwave radiation on the textural properties of layered double hydroxides. Micropor. Mesopor. Mater. 94, 148–158.

Boukhalfa, N., Boutahala, M., Djebri, N., 2017. Synthesis and characterization of ZnAl-layered double hydroxide and organo-K10 montmorillonite for the removal of diclofenac from aqueous solution. Adsorpt. Sci. Technol. 35, 20–36.

Brindley, G.W., Kao, C.-C., 1984. Structural and IR relations among brucite-like divalent metal hydroxides. Phys. Chem. Miner.10, 187–191.

Caminada, D., Escher, C., Fent, K., 2006. Cytotoxicity of pharmaceuticals found in aquatic systems: comparison of PLHC-1 and RTG-2 fish cell lines. Aquat. Toxicol. 79, 114–123.

Carmona, E., Andreu, V., Picó, Y., 2014. Occurrence of acidic pharmaceuticals and personal care products in Turia river basin: from waste to drinking water.Sci. Total Environ. 484, 53–63.

Castro, C.S., Cardoso, D., Nascente, P.A.P., Assaf, J.M., 2011. MgAlLi mixed oxides derived from hydrotalcite for catalytic transesterification. Catal. Lett. 141, 1316–1323.

Cavani, A.V.F., Trifiro, F., 1991. Hydrotalcite-type anionic clays: preparation, properties and applications. Catal. Today 11, 173–301.

Chu, K.H., 2002. Removal of copper from aqueous solution by chitosan in Prawn Shell: adsorption equilibrium and kinetics. J. Hazard. Mater. 90, 77–95.

Commission Implementing Regulation (EU) 2015/495 of 20 March 2015 establishing a watch list of substances for Union-wide monitoring in the field of water policy pursuant to Directive 2008/105/EC of the European Parliament and of the Council, Official Journal of the European Union, 24.3.2015, L78/40 - L78/42.

Conterosito, E., Croce, G., Palin, L., Pagano, C., Perioli, L., Viterbo, D., Boccaleri, E., Paul, G., Milanesio, M., 2013. Structural characterization and thermal and chemical stability of bioactive molecule-hydrotalcite (LDH) nanocomposites. Phys. Chem. Chem. Phys. 15, 13418–13433.

Costantino, U., Leroux, F., Nocchetti, M., Mousty, C., 2013. LDH in physical, chemical, biochemical, and life sciences. In Bergaya, F., Lagaly, G. (Eds.) Handbook of Clay Science, Second Edition, Part B. Elsevier (Chapter 6).

Eades, C., Waring, C.P., 2010. The effects of diclofenac on the physiology of the green shore crab carcinus maenas. Mar. Environ. Res. 69, S46–S48.

Elhalil, A., Farnane, M., Machrouhi, A., Mahjoubi, F.Z., Elmoubarki, R., Tounsadi, H., Abdennouri, M., Barka, N., 2018. Effects of molar ratio and calcination temperature on the adsorption performance of Zn/Al layered double hydroxide nanoparticles in the removal of pharmaceutical pollutants. J. Sci. Adv. Mater. Devices 3, 188–195.

European Waste Catalogue and Hazardous Waste List, Environmental Protection Agency, 2002.

Feito, R., Valcárcel, Y., Catalá, M., 2012. Biomarker assessment of toxicity with miniaturised bioassays: diclofenac as a case study. Ecotoxicology 21, 289–296.

Fraccarollo, A., Cossi, M., Marchese, L., 2010. DFT simulation of Mg/Al hydrotalcite with different intercalated anions: periodic structure and solvating effects on the iodide/triiodide redox couple. Chem. Phys. Lett. 494, 274–278.

Frost, R.L., Martens, W.N., Erickson, K.L., 2005. Thermal decomposition of the hydrotalcite: thermogravimetric analysis and hot stage Raman spectroscopic study. J. Therm. Anal. Calorim. 82, 603–608.

Gao, Z., Du, B., Zhang, G., Gao, Y., Li, Z., Zhang, H., Duan, X., 2011. Adsorption on pentachlorophenol from aqueous solution on dodecylbenzenesulfonate modified

nickel-tianium layered double hydroxide nanocomposites. Ind. Eng. Chem. Res. 50, 5334–5345.

Gil, A., Korili, S.A., 2016. Management and valorization of aluminum saline slags: current status and future trends. Chem. Eng. J. 289, 74–84.

Gil, A., García, A.M., Fernández, M., Vicente, M.A., González–Rodríguez, B., Rives, V., Korili, S.A., 2017. Effect of dopants on the structure of titanium oxide used as a photocatalyst for the removal of emergent contaminants. J. Ind. Eng. Chem. 53, 183-191.

Gil, A., Arrieta, E., Vicente, M.A., Korili, S.A., 2018. Synthesis and CO_2 adsorption properties of hydrotalcite-like compounds prepared from aluminum saline slag wastes. Chem. Eng. J. 334, 1341–1350.

Gil, A., Taoufik, N., García, A.M., Korili, S.A., 2019. Comparative removal of emerging contaminants from aqueous solution by adsorption on an activated carbon. Environ. Technol. 40, 3017-3030.

Giles, C.H., Smith, D., Huitson, A., 1974. A general treatment and classification of the solute adsorption isotherm. I. Theoretical. J. Colloid Interf. Sci. 47, 755-765.

Ginebreda, A., Muñoz, I., de Alda, M.L., Brix, R., López-Doval, J., Barceló, D., 2010. Environmental risk assessment of pharmaceuticals in rivers: relationships between hazard indexes and aquatic macroinvertebrate diversity indexes in the Llobregat river (NE Spain). Environ. Int. 36, 153–162.

Goh, K.H., Lim, T.T., Dong, Z., 2008. Application of layered double hydroxides for removal of oxyanions: a review. Water Res. 42, 1343–1368.

Gomes Silva, C., Bouizi, Y., Fornés, V., García, H., 2009. Layered double hydroxides as highly efficient photocatalysts for visible light oxygen generation from water. J. Am. Chem. Soc. 131, 13833–13839.

Gualandi, I., Scavetta, E., Zappoli, S., Tonelli, D., 2011. Electrocatalytic oxidation of salicylic acid by a cobalt hydrotalcite-like compound modified Pt electrode. Biosens. Bioelectron. 26, 3200–3206.

Haap, T., Triebskorn, R., Köhler, H.R., 2008. Acute effects of diclofenac and DMSO to Daphnia Magna: immobilisation and hsp70-Induction. Chemosphere 73, 353–359.

Hadnadjev-Kostic, M., Vulic, T., Ranogajec, J., Marinkovic-Neducin, R., Radosavljevic-Mihajlovic, A., 2013. Thermal and photocatalytic behavior of Ti/LDH nanocomposites. J. Therm. Anal. Calorim. 111, 1155–1162.

Haraketi, M., Hosni, K., Srasra, E., 2016. Intercalation of salicylic acid into ZnAl and MgAl layered double hydroxides for a controlled release formulation. Colloid J. 78, 533–541.

Heraldy, E., Suprihatin, R.W., Pranoto, 2016. Intercalation of diclofenac in modified Zn/Al hydrotalcite-like preparation. IOP Conf. Series Mater. Sci. Eng. 107, 012026.

Khatem, R., Real Ojeda, M., Bakhti, A., 2015. Use of synthetic clay for removal of diclofenac anti-inflammatory. Eurasian J. Soil Sci. 4, 126–136.

Khraisheh, M.A.M., Al-Degs, Y.S., Allen, S.J., Ahmad, M.N., 2002. Elucidation of controlling steps of reactive dye adsorption on activated carbon. Ind. Eng. Chem. Res. 41, 1651–1657.

Khenniche, L., Aissani, F., 2010. Preparation and characterization of carbons from coffee residue: adsorption of salicylic acid on the prepared carbons. J. Chem. Eng. Data 55, 728–734.

Kikhtyanin, O., Tišler, Z., Velvarská, R., Kubička, D., 2017. Reconstructed Mg-Al hydrotalcites prepared by using different rehydration and drying time: physico-chemical properties and catalytic performance in aldol condensation. Appl. Catal. A Gen. 536, 85–96.

Kosma, C.I., Lambropoulou, D.A., Albanis, T.A., 2014. Investigation of PPCPs in wastewater treatment plants in Greece: occurrence, removal and environmental risk assessment. Sci. Total Environ. 466–467, 421–438.

Krammer, C., 2011. *Aluminum Handbook, Vol. 1: Fundamentals and Materials*;Verlag: Beuth.

Li, C., Wei, M., Evans, D.G., Duan, X., 2014. Layered double hydroxide-based nanomaterials as highly efficient catalysts and adsorbents. Small 10, 4469–4486.

Lowell, S., Shields, J.E., Thomas, M.A., Thommes, M. (Eds.), 2004.Characterization of Porous Solids and Powders: Surface Area, Pore Size and Density, Kluwer Academic Publishers: New York.

Lozano, R.P., Rossi, C., La Iglesia, Á., Matesanz, E., 2012. Zaccagnaite-3R, a new Zn-Al hydrotalcite polytype from El Soplao Cave (Cantabria, Spain). Am. Mineral. 97, 513–523.

Lu, R., Xu, X., Chang, J., Zhu, Y., Xu, S., Zhang, F., 2012. Improvement of photocatalytic activity of TiO_2 nanoparticles on selectively reconstructed layered double hydroxide. Appl. Catal. B Environ. 111–112, 389–396.

Luo, Y., Guo, W., Ngo, H.H., Nghiem, L.D., Hai, F.I., Zhang, J., Liang, S., Wang, X.C., 2014. A review on the occurrence of micropollutants in the aquatic environment and their fate and removal during wastewater treatment. Sci. Total Environ. 473–474, 619–641.

Mendoza-Damián, G., Tzompantzi, F., Mantilla, A., Barrera, A., Lartundo-Rojas, L., 2013. Photocatalytic degradation of 2,4-dichlorophenol with MgAlTi mixed oxides catalysts obtained from layered double hydroxides. J. Hazard. Mater. 263, 67-72.

Mohapatra, L., Parida, K., 2016. A review on the recent progress, challenges and perspective of layered double hydroxides as promising photocatalysts. J. Mater. Chem. A 4, 10744–10766.

Mompelat, S., Le Bot, B., Thomas, O., 2009. Occurrence and fate of pharmaceutical products and by-products, from resource to drinking water. Environ. Int. 35, 803–814.

Mosangi, D., Moyo, L., Kesavan Pillai, S., Ray, S.S., 2016. Acetyl salicylic acid-ZnAl layered double hydroxide functional nanohybrid for skin care application. RSC Advances 6, 105862–105870.

Moulder, J.F., 1992. Handbook of X-Ray Photoelectron Spectroscopy: A Reference Book of Standard Spectra for Identification and Interpretation of XPS Data. Chastain, J. (Ed.) Physical Electronics Division, Perkin-Elmer Corporation.

Nassef, M., Kim, S.G., Seki, M., Kang, I.J., Hano, T., Shimasaki, Y., Oshima, Y., 2010. In ovo nanoinjection of triclosan, diclofenac and carbamazepine affects embryonic development of medaka fish (Oryzias latipes). Chemosphere 79, 966–973.

Poulopoulos, S., Vassilis, I. (Eds), 2006. Adsorption, Ion Exchange and Catalysis - Design of Operations and Environmental Applications, 1st Edition, Elsevier.

Quinn, B., Schmidt, W., O'Rourke, K., Hernan, R., 2011. Effects of the pharmaceuticals

gemfibrozil and diclofenac on biomarker expression in the zebra mussel (Dreissena polymorpha) and their comparison with standardised toxicity tests. Chemosphere 84, 657–663.

Radjenović, J., Petrović, M., Ventura, F., Barceló, D., 2008. Rejection of pharmaceuticals in nanofiltration and reverse osmosis membrane drinking water treatment. Water Res. 42, 3601–3610.

Rives, V., Del Arco, M., Martin, C., 2014. Intercalation of drugs in layered double hydroxides and their controlled release: a review. Appl. Clay Sci. 88–89, 239–269.

Santamaría, L., Vicente, M.A., Korili, S.A., Gil, A. Effect of the preparation method and metal content on the synthesis of metal modified titanium oxide used for the removal of salicylic acid under UV light. Environ. Technol. (in press, DOI: 10.1080/09593330.2018.1555285).

San Román, M.S., Holgado, M.J., Salinas, B., Rives, V., 2012. Characterisation of diclofenac, ketoprofen or chloramphenicol succinate encapsulated in layered double hydroxides with the hydrotalcite-type structure. Appl. Clay Sci. 55, 158–163.

Shao, M., Han, J., Wei, M., Evans, D.G., Duan, X., 2011. The synthesis of hierarchical Zn-Ti layered double hydroxide for efficient visible-light photocatalysis. Chem. Eng. J. 186, 519–524.

Silion, M., Hritcu, D., Popa, M.I., 2009. Intercalation of salicylic acid into ZnAl layered double hydroxides by ion-exchange and coprecipitation method. J. Optoelectron. Adv. Mater. 11, 528–534.

Simonin, J.P., 2016. On the comparison of pseudo-first order and pseudo-second order rate laws in the modeling of adsorption kinetics. Chem. Eng. J. 300, 254–263.

Suarez, S., Lema, J.M., Omil, F., 2009. Pre-treatment of hospital wastewater by coagulation-flocculation and flotation. Bioresour. Technol. 100, 2138–2146.

Theiss, F.L., Ayoko, G.A., Frost, R.L., 2013. Thermogravimetric analysis of selected layered double hydroxides. J. Therm. Anal. Calorim. 112, 649–657.

Thomas, H.C., 1944. Heterogeneous ion exchange in a flowing system. J. Am. Chem. Soc. 66, 1664–1666.

Thommes, M., Kaneko, K., Neimark, A.V., Olivier, J.P., Rodriguez-Reinoso, F., Rouquerol, J., Sing, K.S.W., 2015. Physisorption of gases, with special reference to the evaluation of surface area and pore size distribution (IUPAC technical report). Pure Appl. Chem. 87, 1051–1069.

Triebskorn, R., Casper, H., Scheil, V., Schwaiger, J., 2007. Ultrastructural effects of pharmaceuticals (carbamazepine, clofibric acid, metoprolol, diclofenac) in rainbow trout (*Oncorhynchus Mykiss*) and common carp (*Cyprinus Carpio*). Anal. Bioanal. Chem. 387, 1405–1416.

Tsakiridis, P.E., 2012. Aluminium salt slag characterization and utilization - A review. J. Hazard. Mater. 217–218, 1–10.

Ulibarri, M.A., Hermosin, M.C., 2001. Layered double hydroxides in water decontamination. In Rives, V. (Ed.) Layered Double Hydroxides: Present and Future. Nova Science Publishers (Chapter 9).

Vulliet, E., Cren-Olivé, C., 2011. Screening of pharmaceuticals and hormones at the regional scale, in surface and groundwaters intended to human consumption. Environ. Pollut. 159, 2929–2934.

Wang, M., Jiang, L., Kim, E.J., Hahn, S.H., 2015. Electronic structure and optical properties of $Zn(OH)_2$: LDA+U calculations and intense yellow luminescence. RSC Advances 5, 87496–87503.

Xia, S.-J., Liu, F.-X., Ni, Z.-M., Xue, J.-L., Qian, P.-P., 2013. Layered double hydroxides as efficient photocatalysts for visible-light degradation of Rhodamine B. J. Colloid Interface Sci. 405, 195–200.

Xie, W., Peng, H., Chen, L., 2006. Calcined Mg-Al hydrotalcites as solid base catalysts for methanolysis of soybean oil. J. Mol. Catal. A Chem. 246, 24–32.

Xiong, T., Yuan, X., Wang, H., Wu, Z., Jiang, L., Leng, L., Xi, K., Cao, X., Zeng, G., 2019. Highly efficient removal of diclofenac sodium from medical wastewater by Mg/Al layered double hydroxide-poly(m-phenylenediamine) composite. Chem. Eng. J. 366, 83–91.

Captions

Table 1. Basal value and interlayer distance of Al* LDH series.

Table 2. Textural properties of the series synthesized with commercial aluminum.

Table 3. Textural properties of the series synthesized with extracted aluminum.

Table 4. Mass losses (%) in the steps indicated from the thermogravimetric analyses of the LDH series.

Table 5. Surface concentration (% atomic) and proposed elemental formula of the calcined compounds of the surface of the LDH.

Table 6. $Zn_6Al^*_2$ adsorption data at various pHs.

Table 7. Freundlich, Langmuir and Toth parameters for the diclofenac adsorption process on $Zn_6Al^*_2$.

Table 8. Thomas model parameters for the fixed-bed column adsorption of drugs on $Zn_6Al^*_2$ without pH modification.

Fig. 1. Powder X ray diffraction patterns of non-calcined (a) and calcined (b) samples synthesized at different pH values, non-calcined (c) and calcined (d) samples synthetized with commercial aluminum and non-calcined (e) and calcined (f) samples synthetized with extracted aluminum.

Fig. 2. Memory effect of $Zn_6Al^*_2$ hydrotalcite. Non-calcined (a), calcined (b), rehydrated (c) and rehydrated with diclofenac (d).

Fig. 3. SEM micrographs and EDX analysis of $Zn_6Al^*_2$ (a), $Zn_6Al^*_{1.5}Ti_{0.5}$ (b), Zn_6AlTi (c), $Zn_6Al_{0.5}Ti_{1.5}$ (d) and $Zn_6 Ti_2$ (e) samples.

Fig. 4. TG and DGT curves of the LDH prepared from commercial aluminum (black) and extracted aluminum (red).

Fig. 5. XPS spectra of Zn 2p (a), O 1s (b), Al 2p (c) and Ti 2p (d) of the calcined Al* series.

Fig. 6. Kinetic data for diclofenac adsorbed on $Zn_6Al^*_2$ (first range), $Zn_6Al^*_{1.5}Ti_{0.5}$ (second range), Zn_6Al^*Ti (third range) and $Zn_6Al^*_{0.5}Ti_{1.5}$ (fourth range) with different amounts of adsorbent (first column) and different drug concentrations

(second column). Adjustments to pseudo-first and second order models are also shown.

Fig. 7. Kinetic data for salicylic acid adsorbed on $Zn_6Al^*_2$ (first range), $Zn_6Al^*_{1.5}Ti_{0.5}$ (second range), Zn_6Al^*Ti (third range) and $Zn_6Al^*_{0.5}Ti_{1.5}$ (fourth range) with different amounts of adsorbent (first column) and different drug concentrations (second column). Adjustments to pseudo-first and second order models are also shown.

Fig. 8. Comparison of the breakthrough curve for diclofenac and salycilic acid in a column with 25 mg of $Zn_6Al^*_2$ and their adjustment to the Thomas model (line).

Table 1. Basal value and interlayer distance of Al* LDH series.

Sample	d(003) (nm)	*c* (nm)	Interlayer height (nm)
$Zn_6Al^*_2$	0.761	2.286	0.291
$Zn_6Al^*_{1.5}Ti_{0.5}$	0.752	2.255	0.281
Zn_6Al^*Ti	0.757	2.270	0.286
$Zn_6Al^*_{0.5}Ti_{1.5}$	0.761	2.282	0.290
Zn_6Ti_2	0.686	2.059	0.215
Rehydrated $Zn_6Al^*_2$	0.734	2.208	0.263
Rehydrated $Zn_6Al^*_2$ with diclofenac	1.097-0.746	3.291-2.238	0.626-0.275

Table 2. Textural properties of the series synthesized with commercial aluminum.

Sample	S_{BET} (m^2/g)	S_{ext}(m^2/g)	$V_{\mu p}$ (cm^3/g)		S_{BET} (m^2/g)	S_{ext} (m^2/g)	$V_{\mu p}$ (cm^3/g)
		Non calcined			*Calcined*		
Zn_6Al_2 pH10	81	61	0.0079		73	73	0
Zn_6AlTi pH10	150	141	0.0025		91	89	0.0002
Zn_6 $Al_{0.5}Ti_{1.5}$ pH10	190	184	0.0008		104	104	0
Zn_6 Ti_2 pH10	184	184	0		95	95	0
$Zn_6Al_{1.5}Ti_{0.5}$ pH10	142	125	0.0061		103	95	0.0030
$Zn_6Al_{1.5}Ti_{0.5}$ pH5	196	196	0		126	126	0
$Zn_6Al_{1.5}Ti_{0.5}$ pH12	67	65	0.0006		59	58	0.0004

Table 3. Textural properties of the series synthesized with extracted aluminum.

Sample	S_{BET} (m^2/g)	S_{ext} (m^2/g)	$V_{\mu p}$ (cm^3/g)	S_{BET} (m^2/g)	S_{ext} (m^2/g)	$V_{\mu p}$ (cm^3/g)
	Non calcined			*Calcined*		
$Zn_6Al^*_2$ pH10	78	69	0.0045	79	69	0.0046
$Zn_6Al^*_{1.5}Ti_{0.5}$ pH10	152	145	0.0027	100	91	0.0041
Zn_6Al^*Ti pH10	152	148	0.0013	93	86	0.0029
$Zn_6Al^*_{0.5}Ti_{1.5}$ pH10	199	199	0	95	89	0.0023
Zn_6Ti_2 pH10	184	184	0	95	95	0

Table 4. Mass losses (%) in the steps indicated from the thermogravimetric analyses of the LDH series.

Sample	1	2	3	4	5	TOTAL (%)
Zn_6Al_2	0-373 K	373-473 K	473-673 K	673-923 K	923-1123 K	
	2.2	12.0	13.1	2.9	1.1	31.52
$Zn_6Al_{1.5}Ti_{0.5}$	0-383 K	383-458 K	458-673 K	673-923 K	923-1123 K	
	5.1	6.0	15.1	2.0	0.6	28.87
Zn_6AlTi	0-403 K	403-673 K	448-673 K	673-923 K	923-1123 K	
	3.0	4.6	13.17	2.0	0.6	23.09
$Zn_6 Al_{0.5}Ti_{1.5}$	0-373 K	373-448 K	448-673 K	673-923 K	923-1123 K	
	2.3	4.2	12.2	1.5	0.3	21.12
$Zn_6 Ti_2$	0-473 K		473-698 K	698-923 K	923-1123 K	
	11.5		10.37	1.4	1.1	24.46

Table 5. Surface concentration (% atomic) and proposed elemental formula of the calcined compounds on the surface of the LDH.

	Zn	**Al**	**O**	**Ti**	**Proposed formula**
$Zn_6Al^*_2$	25.6	10.4	55.9	--	$Zn_6Al^*_{2.4}$
$Zn_6Al^*_{1.5}Ti_{0.5}$	25	8.6	56	1.5	$Zn_6Al^*_{2.1}Ti_{0.4}$
Zn_6Al^*Ti	25.8	5.2	56.5	4.4	$Zn_6Al^*_{1.2}Ti_{1.0}$
$Zn_6Al^*_{0.5}Ti_{1.5}$	26.8	3.1	55.1	5.9	$Zn_6Al^*_{0.7}Ti_{1.3}$
Zn_6Ti_2	26.5	--	56.1	9	$Zn_6Ti_{2.0}$

Table 6. $Zn_6Al^*_2$ adsorption data at various pH values.

pH	q_t **(diclofenac)** (**μmol**/g)	**pH**	q_t **(salicylic acid)** (**μmol**/g)
		2	3
2	unstable	**2.7**	19
4.2	108	**4**	13
6	72	**6**	4
8	40	**8**	0.4
10	no adsorption	**10**	no adsorption

Table 7. Freundlich, Langmuir and Toth parameters for the diclofenac adsorption process on $Zn_6Al^*_2$.

Freundlich		**Langmuir**		**Toth**	
q_F	58.8	q_L (μmol/g)	1172	q_T (μmol/g)	3036
m_F	3.01	k_L (mL/μmol)	0.015	k_T (mL/μmol)	0.114
χ^2	3623	χ^2	7490	m_T	0.27
R	0.98	**R**	0.96	χ^2	2392
				R	0.98

Table 8. Thomas model parameters for the fixed-bed column adsorption of drugs on $Zn_6Al^*_2$ without pH modification.

	Diclofenac	**Salicylic acid**
k_{Th} (mL/min·μmol)	0.035	0.008
q_{ads} (μmol/g)	1157	4597
χ^2	1.03	0.094
R	0.96	0.98
m	0.0264	0.0264

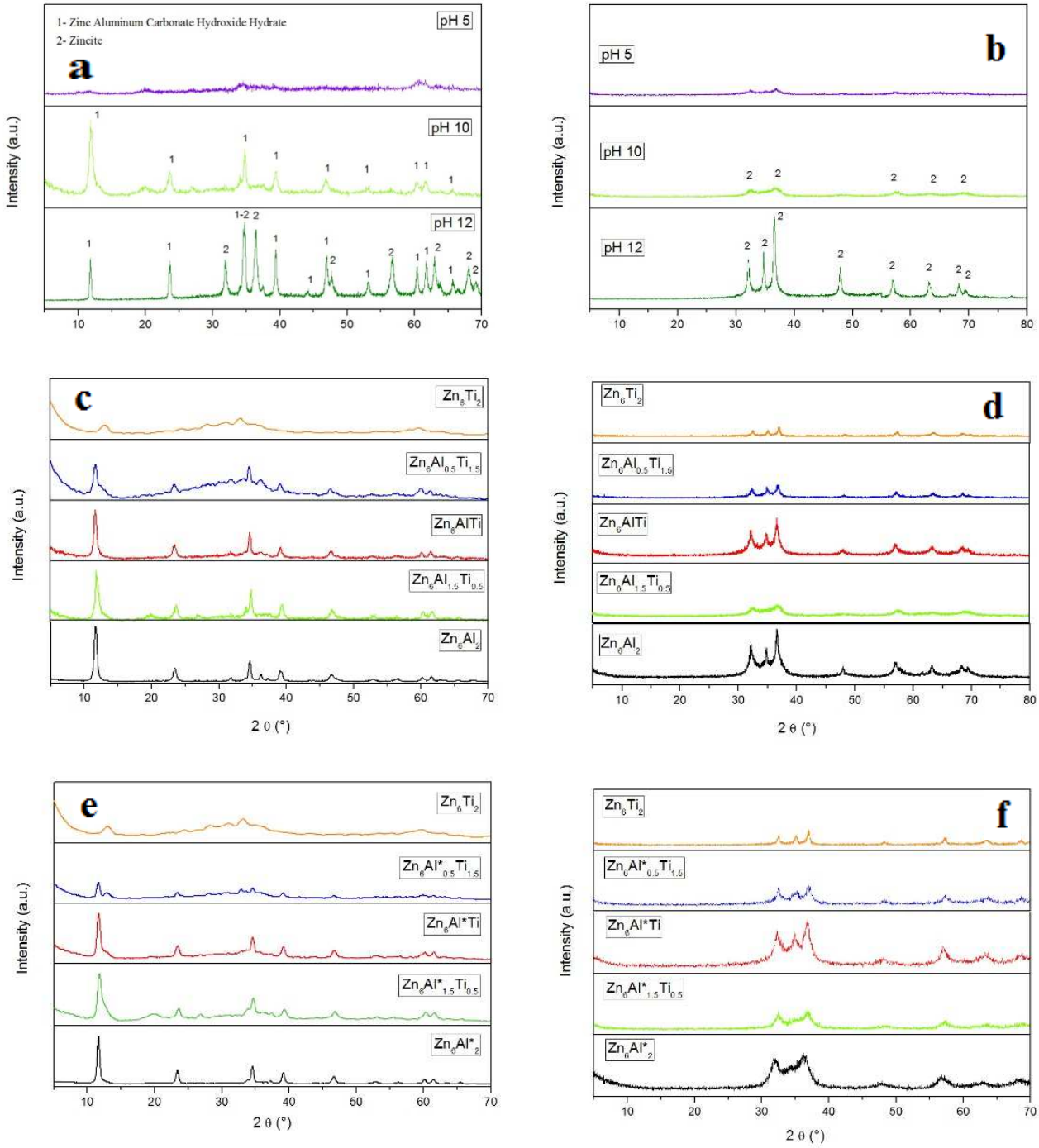

Fig. 1. Powder X ray diffraction patterns of non-calcined (a) and calcined (b) samples synthesized at various pH values, non-calcined (c) and calcined (d) samples synthesized with commercial aluminum and non-calcined (e) and calcined (f) samples synthesized with extracted aluminum.

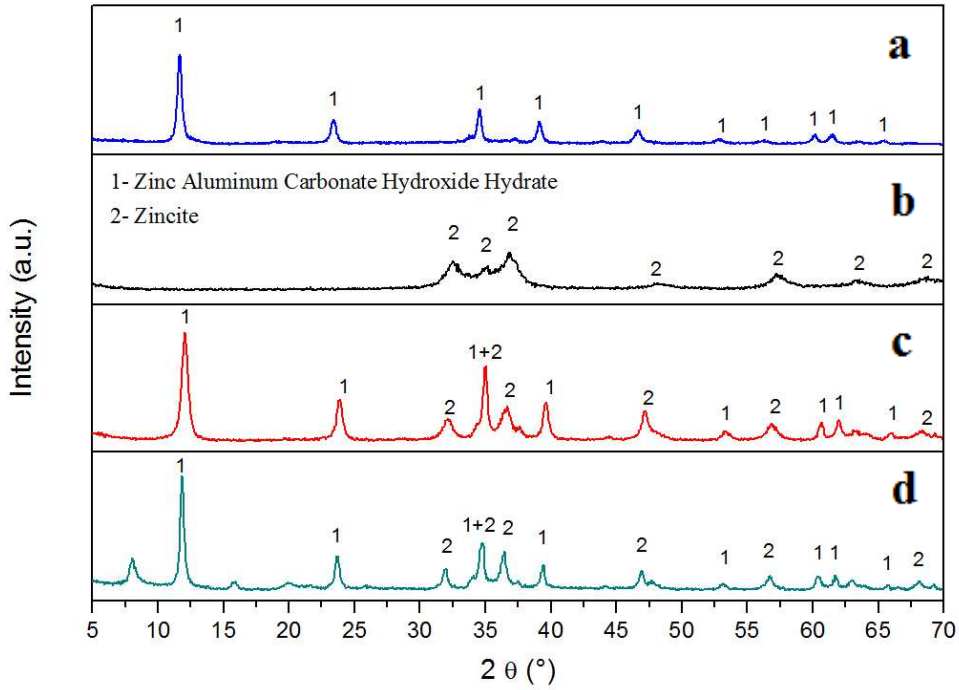

Fig. 2. Memory effect of $Zn_6Al^*_2$hydrotalcite. Non-calcined (a), calcined (b), rehydrated (c) and rehydrated with diclofenac (d).

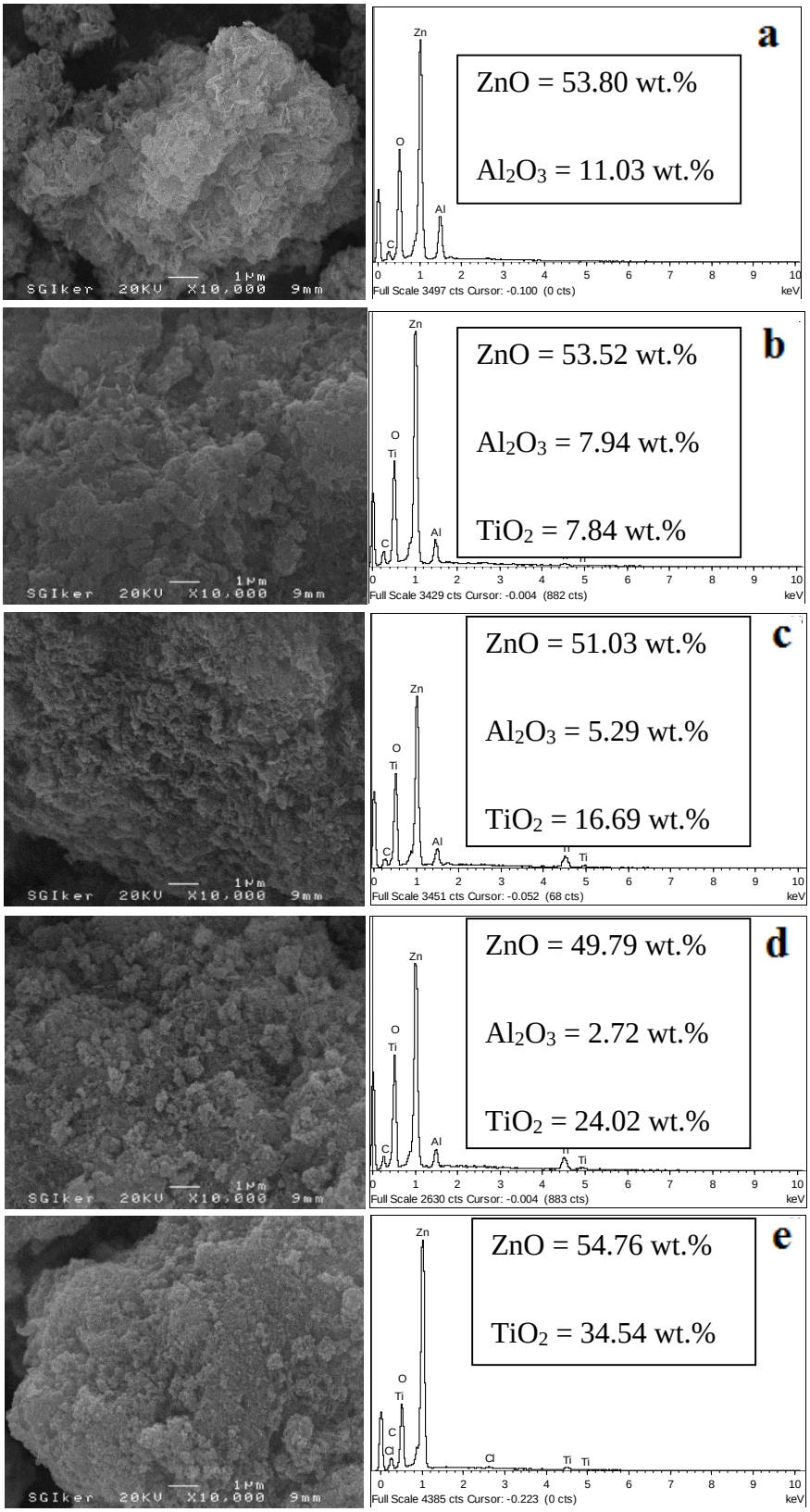

Fig. 3. SEM micrographs and EDX analysis of $Zn_6Al^*_2$ (a), $Zn_6Al^*_{1.5}Ti_{0.5}$ (b), Zn_6AlTi (c), $Zn_6Al_{0.5}Ti_{1.5}$ (d) and Zn_6Ti_2 (e) samples.

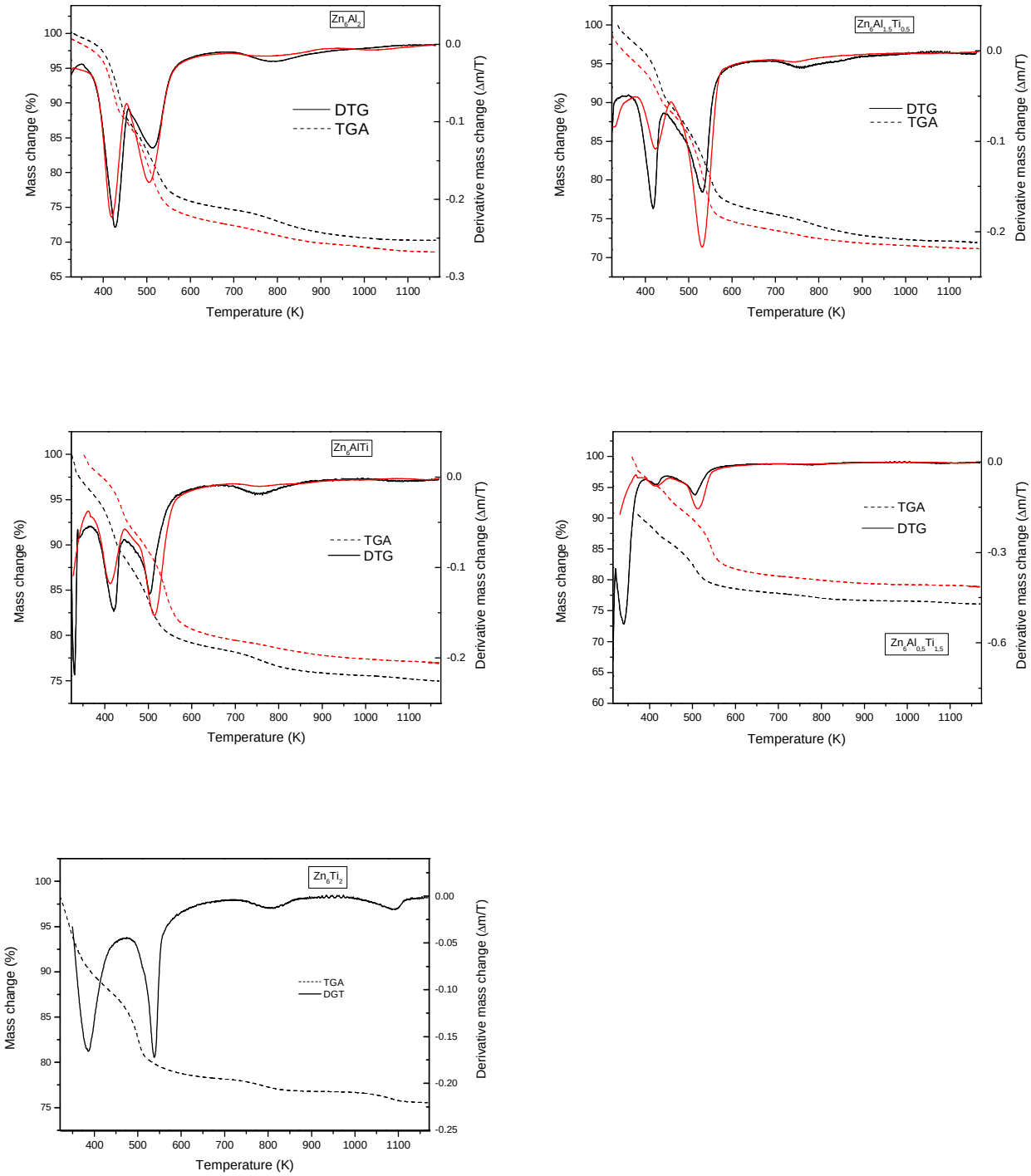

Fig. 4. TG and DTG curves of the LDH prepared from commercial aluminum (black) and extracted aluminum (red).

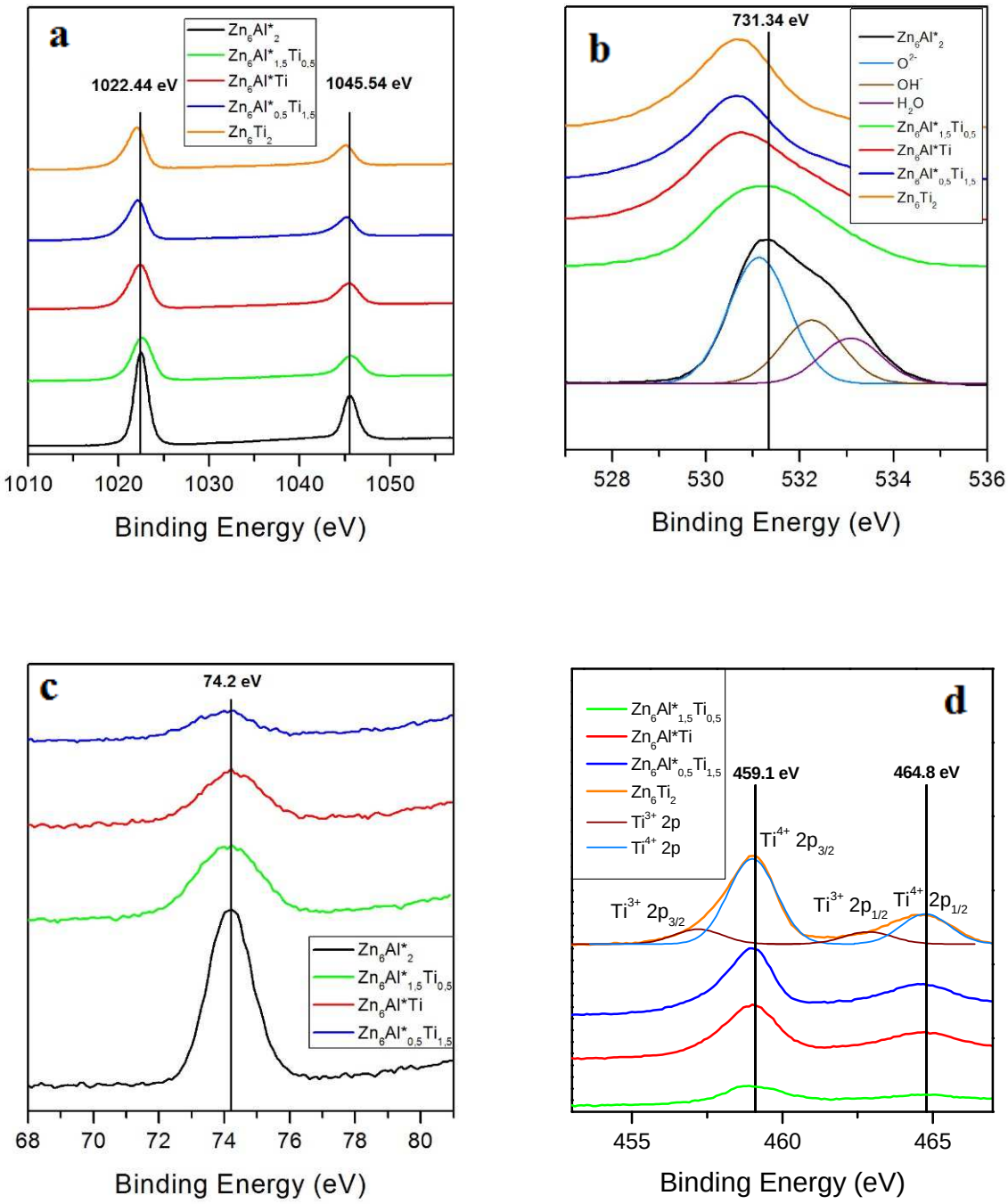

Fig. 5. XPS spectra of Zn 2p (a), O 1s (b), Al 2p (c) and Ti 2p (d) of the calcined Al* series.

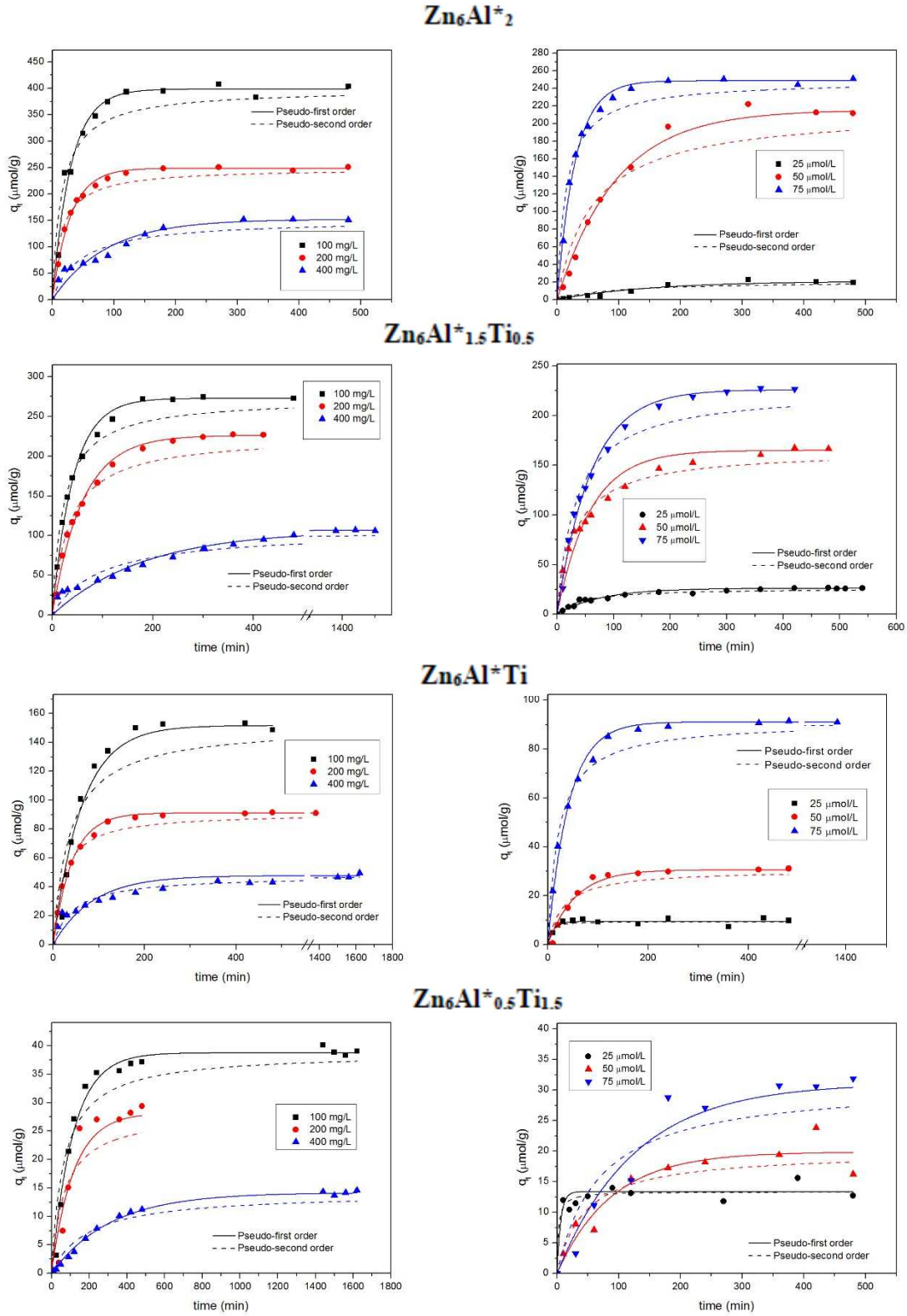

Fig. 6. Kinetic data for diclofenac adsorbed on $Zn_6Al^*_2$ (first range), $Zn_6Al^*_{1.5}Ti_{0.5}$ (second range), Zn_6Al^*Ti (third range) and $Zn_6Al^*_{0.5}Ti_{1.5}$ (fourth range) with different amounts of adsorbent (first column) and different drug concentrations (second column). Adjustments to pseudo-first and second order models are also shown.

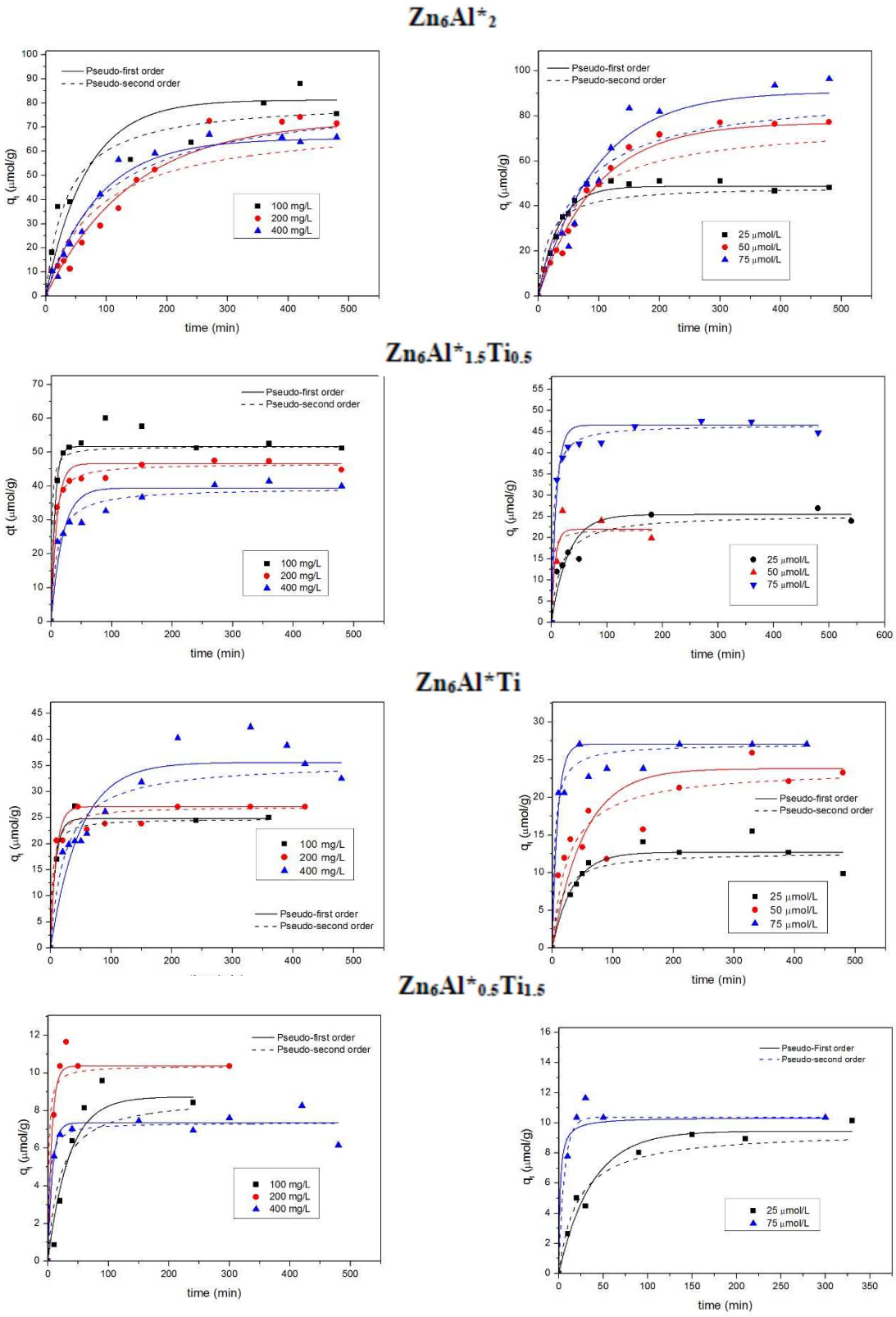

Fig. 7. Kinetic data for salicylic acid acid adsorbed on $Zn_6Al^*_2$ (first range), $Zn_6Al^*_{1.5}Ti_{0.5}$ (second range), Zn_6Al^*Ti (third range) and $Zn_6Al^*_{0.5}Ti_{1.5}$ (fourth range) with different amounts of adsorbent (first column) and different drug concentrations (second column). Adjustments to pseudo-first and second order models are also shown.

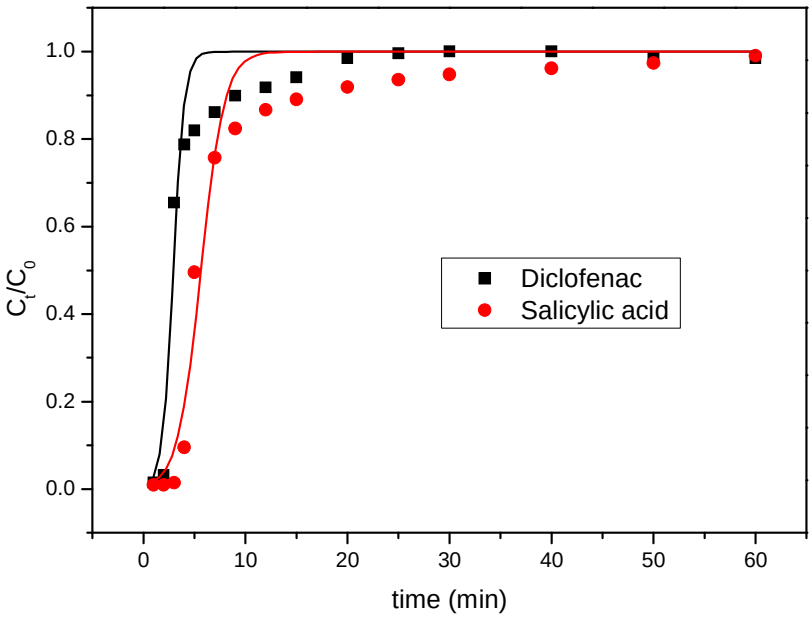

Fig. 8. Comparison of the breakthrough curve for diclofenac and salycilic acid in a column with 25 mg of $Zn_6Al^*_2$ and their adjustment to the Thomas model (line).